

Showcasing research from Pengqiang Yan and Prof. Wei Qi at the Institute of Metal Research, Chinese Academy of Sciences, China.

Methanol oxidative dehydrogenation and dehydration on carbon nanotubes: active sites and basic reaction kinetics

Carbon nanotubes were applied for the first time to the methanol conversion reaction showing the advantage of low CO_2 selectivity and long term stability. The active sites and kinetics for both dehydration and oxidative dehydrogenation reactions were revealed via chemical titration, model catalysts and structure-activity analysis.

As featured in:



See Wei Qi *et al.*,
Catal. Sci. Technol., 2020, 10, 4952.

COMMUNICATION

[View Article Online](#)
[View Journal](#) | [View Issue](#)Cite this: *Catal. Sci. Technol.*, 2020, 10, 4912Received 26th March 2020,
Accepted 15th May 2020

DOI: 10.1039/d0cy00600a

rsc.li/catalysisLong wavelength visible light-responsive SrTiO₃ photocatalysts doped with valence-controlled Ru for sacrificial H₂ and O₂ evolution†Sho Suzuki,^a Akihide Iwase ^{ab} and Akihiko Kudo ^{*ab}

SrTiO₃ doped with Ru, H₂-reduced SrTiO₃ doped with Ru and SrTiO₃ codoped with Ru and Sb were developed as active photocatalysts for sacrificial H₂ and O₂ evolution under visible light irradiation. H₂-Reduced SrTiO₃:Ru showed the highest activity responding up to 750 nm, almost the whole range of visible light.

Photocatalytic water splitting is a promising chemical reaction to convert solar energy into storable chemical energy, so-called artificial photosynthesis.^{1–6} Utilization of visible light is a key issue to achieve highly efficient solar energy conversion. Accordingly, development of photocatalysts with responses to a wide range of visible light is an important research topic.

Doping of metal ions is a useful technique to make materials responsive to light with longer wavelengths.^{2,7} The doped metal ions form impurity levels in the forbidden band of the host material, and hence new energy gaps appear in addition to the band gap of the host material. For example, Rh-doped SrTiO₃ is an established photocatalyst which is highly active for sacrificial H₂ evolution under visible light irradiation.⁸ In addition to Rh ions, Cr, Ir, and Ni ions are known as effective dopants.^{9–13} We have preliminarily reported that Ru-doped SrTiO₃ shows photocatalytic activities for sacrificial H₂ and O₂ evolution under visible light irradiation.⁸ However, the details of the photocatalytic properties and the band structure have not been clarified yet. It is important to improve the Ru-doped SrTiO₃ by some modifications.

Codoping with a second dopant can control the oxidation number of the main dopant. For example, Rh ions are mainly

doped as Rh⁴⁺ at Ti⁴⁺ sites when only Rh is doped into SrTiO₃.¹⁴ In contrast, the oxidation number of the rhodium species is controlled from Rh⁴⁺ to Rh³⁺ by codoping of Sb⁵⁺ into SrTiO₃ to maintain the charge balance, according to 2Ti⁴⁺ = Rh³⁺ + Sb⁵⁺.^{15,16} As a result, Rh,Sb-codoped SrTiO₃ shows activity for water splitting under visible light irradiation,¹⁶ being different from Rh-doped SrTiO₃. Thus, the oxidation number of the doped metal ions drastically affects the photocatalytic properties.

In the present study, we investigated the photocatalytic properties of Ru-doped SrTiO₃ to develop and improve a photocatalyst responding to long wavelength visible light. Sb-Codoping and H₂-reduction were applied to Ru-doped SrTiO₃ to control the oxidation number of doped Ru. The band structures of Ru-doped SrTiO₃, Ru,Sb-codoped SrTiO₃, and Ru-doped SrTiO₃ after H₂ reduction were also discussed.

Metal ion-doped SrTiO₃ was prepared by a solid-state reaction. The starting materials SrCO₃ (Kanto Chemical, 99.9%), TiO₂ (Soekawa Chemical, 99.9%), RuO₂ (Rare Metallic, 99.9%), Sb₂O₅ (Nakarai Tesque, 98%), Nb₂O₅ (Kojundo Chemical, 99.99%) and Ta₂O₅ (Rare Metallic, 99.99%) were mixed in atomic ratios of Sr/Ti/Ru = 1.015:0.997:0.003 for Ru(0.3%)-doped SrTiO₃, Sr/Ti/Ru/Sb = 1.015:0.9925:0.003:0.0045 for Ru(0.3%),Sb(0.45%)-codoped SrTiO₃, and Sr/Ti/Ru/M = 1.015:0.991 – x:0.003:0.006 for Ru(0.3%),Nb(0.6%)- and Ru(0.3%),Ta(0.6%)-codoped SrTiO₃. The mixture was calcined in an alumina crucible at 1273 K for 10 h. H₂-Reduced SrTiO₃ doped with Ru was prepared by reduction in one atmosphere of H₂ at 473 K or 673 K for 2 h. The crystal phase of the prepared powder was analyzed on an X-ray diffractometer (Rigaku, MiniFlex) using CuKα radiation. Diffuse reflectance spectra were obtained using a UV-vis-NIR spectrometer (JASCO, Ubest-570) equipped with an integrating sphere and were converted from reflection to K–M function by the Kubelka–Munk method. Electron spin resonance (ESR) spectra were recorded at 77 K on an ESR spectrometer (JEOL, JES-FA200).

Photocatalytic reactions of sacrificial H₂ and O₂ evolution were carried out using a gas-tight circulation system with a

^a Department of Applied Chemistry, Faculty of Science, Tokyo University of Science, 1-3 Kagurazaka, Shinjuku-ku, Tokyo 162-8601, Japan. E-mail: a-kudo@rs.tus.ac.jp

^b Photocatalysis International Research Center, Research Institute for Science and Technology, Tokyo University of Science, 2641 Yamazaki, Noda-shi, Chiba 278-8510, Japan

† Electronic supplementary information (ESI) available: XRD patterns of the photocatalysts. See DOI: 10.1039/d0cy00600a



top-irradiation cell with a Pyrex window. Photocatalyst powder (0.2 g) was dispersed in an aqueous solution (120 mL) containing 10 vol% methanol as a hole scavenger and a certain amount of H_2PtCl_6 as a source of a Pt cocatalyst for sacrificial H_2 evolution. Photocatalyst powder (0.2 g) was dispersed in an aqueous solution (120 mL) containing 20 mmol L^{-1} AgNO_3 as an electron scavenger for sacrificial O_2 evolution. The suspension was irradiated with visible light using a 300 W Xe lamp (PerkinElmer, Cermex PE300BF) with a long-pass filter (HOYA L42). The amounts of evolved gases were determined using an online gas chromatograph (Shimadzu, GC-8A, MS-5A column, TCD, Ar carrier). The apparent quantum yield (AQY) for the sacrificial O_2 evolution was estimated using the following equation.

$$\begin{aligned} [\text{AQY}\%] &= 100 \times [\text{the number of reacted holes}] / \\ &\quad [\text{the number of incident photons}] \\ &= 100 \times [\text{the number of evolved } \text{O}_2 \text{ molecules}] \times 4 / \\ &\quad [\text{the number of incident photons}] \end{aligned}$$

The photon flux of the monochromatic light through the band-pass filters (Asahi Spectra, MAX-303) was measured using a silicon diode head (Ophir Optronics, PD300-UV head and NOVA display).

XRD measurements revealed that Ru(0.3%)-doped SrTiO_3 ($\text{SrTiO}_3\text{:Ru}$) was obtained without noticeable impurities (Fig. S1†), indicating that Ru ions were doped into the SrTiO_3 lattice. Judging from the ionic radii of Ru^{3+} (68 pm, 6 coordination) and Ru^{4+} (62 pm, 6 coordination) compared to that of Ti^{4+} (60.5 pm, 6 coordination),¹⁷ the Ru ions should be doped at Ti^{4+} sites. In the ESR measurements, no signal was observed for non-doped SrTiO_3 , while Ru-doped SrTiO_3 gave a small signal, as shown in Fig. 1. The intensity of the signal increased by H_2 -reduction and Sb-codoping, indicating that the observed ESR signal was from either Ti^{3+} or Ru^{3+} . Upon considering the stability of SrTiO_3 , Ti^{3+} may not be formed by H_2 reduction at 673 K. Thus, we can conclude that Ru was mainly doped as Ru^{4+} which is ESR inactive and was reduced to Ru^{3+} by H_2 -reduction and Sb-codoping.

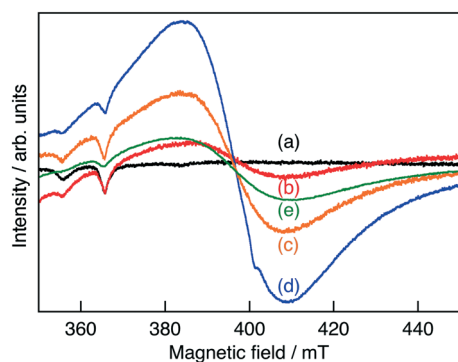


Fig. 1 ESR spectra for Ru^{3+} in (a) non-doped SrTiO_3 , (b) $\text{SrTiO}_3\text{:Ru}$ (0.3%), $\text{SrTiO}_3\text{:Ru}$ (0.3%) after H_2 -reduction at (c) 473 K and (d) 673 K and (e) $\text{SrTiO}_3\text{:Ru}$ (0.3%),Sb(0.45%).

The change in the oxidation number of a dopant, especially a transition metal cation with d^n configuration ($n = 1-9$), usually affects the photoabsorption properties of the material, as observed for Rh-doped SrTiO_3 and Ir-doped SrTiO_3 .¹³⁻¹⁶ $\text{SrTiO}_3\text{:Ru}$ possessed a wide absorption band in the visible light region in addition to the band gap absorption of the SrTiO_3 host (Fig. 2b). Upon reduction with H_2 , the absorption at around 500–700 nm increased, while the absorption at around 400–450 nm decreased (Fig. 2c and d). On the basis of the change in the absorption profile, the absorption bands at around 500–700 nm and 400–450 nm were assigned to Ru^{3+} - and Ru^{4+} -related transitions, respectively. This behavior corresponded to the change in ESR signals.

Sb, Nb and Ta ions were codoped with Ru into SrTiO_3 to control the Ru to be trivalent. The XRD patterns of Ru,Sb-, Ru,Nb- and Ru,Ta-codoped SrTiO_3 were the same as that of $\text{SrTiO}_3\text{:Ru}$ (Fig. S1†), indicating the successful doping of Sb, Nb and Ta. Upon codoping with Sb ions, the absorption in the diffuse reflectance spectrum at around 500–800 nm increased, whereas the absorption at around 400–450 nm decreased (Fig. 2e). This is because the doped Ru ions were controlled to be trivalent by codoping with Sb ions. In more detail, two Ti^{4+} ions were substituted with Ru^{3+} and Sb^{5+} ions to maintain the charge balance, according to $2\text{Ti}^{4+} = \text{Ru}^{3+} + \text{Sb}^{5+}$. Actually, the intensity of the ESR signal also increased by codoping with Sb ions (Fig. 1e). However, the intensities of the absorption at around 500–800 nm in the diffuse reflectance spectra and the ESR signal were lower than those of the sample after H_2 -reduction. These lower intensities indicate that Ru^{4+} ions still existed even in Ru,Sb-codoped SrTiO_3 . The profile of the diffuse reflectance spectrum of $\text{SrTiO}_3\text{:Ru}$ did not change upon codoping of either Nb or Ta ions (Fig. 2f and g). This indicates that the Nb and Ta ions do not contribute to control of the oxidation number of the doped Ru ions, being different from Sb ions. The codopants should locate close to the Ru ions to maintain the charge balance. Both Ru^{3+} (68 pm, 6 coordination) of the dopant and Nb^{5+} or Ta^{5+} (64 pm, 6 coordination) of the codopants

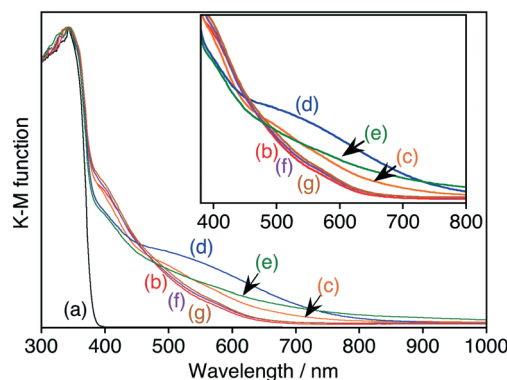


Fig. 2 Diffuse reflectance spectra of (a) non-doped SrTiO_3 , (b) $\text{SrTiO}_3\text{:Ru}$ (0.3%), $\text{SrTiO}_3\text{:Ru}$ (0.3%) after H_2 -reduction at (c) 473 K and (d) 673 K, (e) $\text{SrTiO}_3\text{:Ru}$ (0.3%),Sb(0.45%), (f) $\text{SrTiO}_3\text{:Ru}$ (0.3%),Nb(0.6%), and (g) $\text{SrTiO}_3\text{:Ru}$ (0.3%),Ta(0.6%).



possess larger ionic radii than Ti^{4+} (60.5 pm, 6 coordination). Therefore, it is unfavourable that Ru^{3+} and Nb^{5+} or Ta^{5+} are closely located to each other. In contrast, Sb^{5+} (60 pm, 6 coordination) possesses a slightly smaller ionic radius than Ti^{4+} (60.5 pm, 6 coordination). This suggests that Sb^{5+} can locate closely to Ru ions resulting in control of the oxidation number of the doped Ru ions compared to Nb and Ta ions.

Table 1 shows the photocatalytic activities for sacrificial H_2 and O_2 evolution over $\text{SrTiO}_3\text{:Ru}$, H_2 -reduced $\text{SrTiO}_3\text{:Ru}$ and codoped $\text{SrTiO}_3\text{:Ru}$ under visible light irradiation. $\text{SrTiO}_3\text{:Ru}$ showed activities for both sacrificial H_2 evolution and O_2 evolution, as previously reported.⁸ H_2 -Reduced $\text{SrTiO}_3\text{:Ru}$ showed a higher activity for the sacrificial O_2 evolution than the pristine $\text{SrTiO}_3\text{:Ru}$ and the activity increased with increasing temperature of H_2 reduction.

In contrast, the activity for the sacrificial H_2 evolution was decreased by H_2 reduction. The H_2 -reduced $\text{SrTiO}_3\text{:Ru}$ continuously produced O_2 under visible light irradiation, as shown in Fig. 3. The turnover number which is the ratio of the number of reacted holes to the number of doped Ru ions is calculated to be 45 using the amount of evolved O_2 (37 μmol for 4 h) and doped Ru ions (3.3 μmol in 0.2 g of $\text{SrTiO}_3\text{:Ru}$). The activity for sacrificial O_2 evolution over Ru,Sb-codoped SrTiO_3 was also higher than that over $\text{SrTiO}_3\text{:Ru}$, while the activity for sacrificial H_2 evolution was lower. This trade-off between the sacrificial H_2 evolution and O_2 evolution for the codoped photocatalyst was similar to that for Rh,Sb-codoped SrTiO_3 .^{15,16} A doped photocatalyst with impurity levels formed by a dopant with an oxidation number stabilized by H_2 -reduction and Sb-codoping is sometimes not suitable for H_2 evolution, as observed for Rh,Sb-codoped SrTiO_3 .^{15,16} Ru,Nb- and Ru,Ta-codoped SrTiO_3 showed similar activities for sacrificial H_2 and O_2 evolution to that of $\text{SrTiO}_3\text{:Ru}$. Thus, the activity for sacrificial O_2 evolution increased upon increasing the rate of doped Ru^{3+} by H_2 reduction and Sb-codoping.

To further understand the relationship between the doped Ru^{3+} ions and the activity for O_2 evolution, action spectra were measured, as shown in Fig. 4. $\text{SrTiO}_3\text{:Ru}$, H_2 -reduced $\text{SrTiO}_3\text{:Ru}$ and Ru,Sb-codoped SrTiO_3 ($\text{SrTiO}_3\text{:Ru,Sb}$) showed activity for sacrificial O_2 evolution using light up to 660 nm

Table 1 Sacrificial H_2 and O_2 evolution over the $\text{SrTiO}_3\text{:Ru}$, H_2 -reduced $\text{SrTiO}_3\text{:Ru}$ and codoped $\text{SrTiO}_3\text{:Ru}$ photocatalysts under visible light irradiation

Photocatalyst ^a	Activity/ $\mu\text{mol h}^{-1}$	
	H_2 ^b	O_2 ^c
$\text{SrTiO}_3\text{:Ru}(0.3\%)$	4.0	4.4
$\text{SrTiO}_3\text{:Ru}(0.3\%)$ with H_2 -red. (473 K)	1.7	8.0
$\text{SrTiO}_3\text{:Ru}(0.3\%)$ with H_2 -red. (673 K)	1.8	16.1
$\text{SrTiO}_3\text{:Ru}(0.3\%),\text{Sb}(0.45\%)$	0.2	7.3
$\text{SrTiO}_3\text{:Ru}(0.3\%),\text{Nb}(0.6\%)$	3.3	3.3
$\text{SrTiO}_3\text{:Ru}(0.3\%),\text{Ta}(0.6\%)$	2.4	4.3

Photocatalyst: 0.2 g; reactant solution: 120 mL; light source: 300 W Xe lamp with a long-pass filter ($\lambda > 420$ nm, L42). ^a Prepared at 1273 K for 10 h by a solid-state reaction with 1.5 at% excess Sr. ^b Pt(0.3 wt%)-Cocatalyst; 10 vol% MeOH aq. ^c 20 mmol L^{-1} AgNO_3 aq.

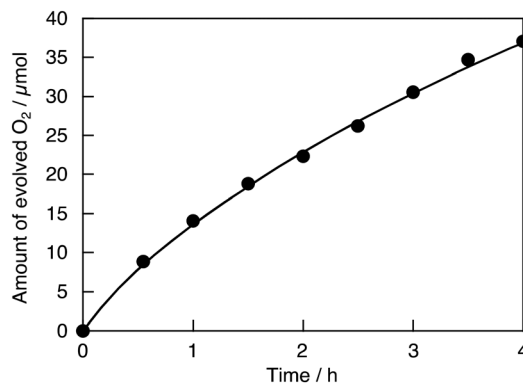


Fig. 3 Photocatalytic O_2 evolution over $\text{SrTiO}_3\text{:Ru}(0.3\%)$ after H_2 -reduction at 673 K from an aqueous AgNO_3 solution under visible light irradiation. Photocatalyst: 0.2 g; reactant solution: 20 mmol L^{-1} AgNO_3 aq., 120 mL; light source: 300 W Xe lamp with a long-pass filter ($\lambda > 420$ nm, L42).

(1.88 eV), 750 nm (1.65 eV) and 670 nm (1.85 eV), respectively.

The onset of the action spectrum for the O_2 evolution over the $\text{SrTiO}_3\text{:Ru}$ in which doped Ru was mainly tetravalent was similar to that of the photoanodic current of an RuO_2 -doped SrTiO_3 photoelectrode, though the condition of the doped Ru was not clear for the photoelectrode.¹⁸ As discussed above, the corresponding absorption bands were assigned to Ru^{3+} -related transitions. The possible band structures of $\text{SrTiO}_3\text{:Ru}$, H_2 -reduced $\text{SrTiO}_3\text{:Ru}$ and $\text{SrTiO}_3\text{:Ru,Sb}$ judging from the action spectra are summarized in Fig. 5. The valence band maximum consisting of the $\text{O}2p$ orbitals of metal oxides is generally located at around +3.0 V vs. NHE at pH 0,¹⁹ and the band levels of metal oxides shift with -0.059 V pH^{-1} . Accordingly, the conduction band minimum and the valence band maximum of SrTiO_3 with a band gap of 3.2 eV are estimated to be at -0.61 V and $+2.59$ V vs. NHE at pH 7, respectively. When the Ru^{3+} -related transition is the

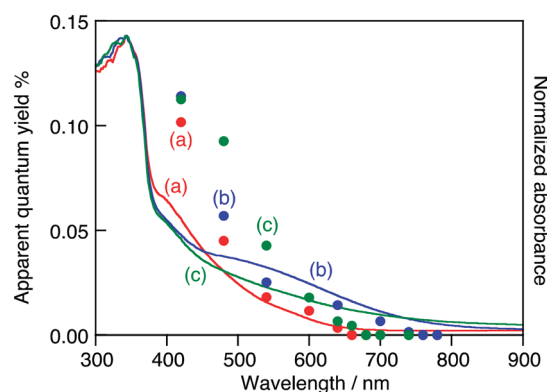


Fig. 4 Action spectra for photocatalytic O_2 evolution from an aqueous AgNO_3 solution (closed circles) and diffuse reflectance spectra (solid lines) of (a) $\text{SrTiO}_3\text{:Ru}(0.3\%)$, (b) $\text{SrTiO}_3\text{:Ru}(0.3\%)$ after H_2 -reduction at 673 K and (c) $\text{SrTiO}_3\text{:Ru}(0.3\%),\text{Sb}(0.45\%)$. Photocatalyst: 0.2 g; reactant solution: 20 mmol L^{-1} AgNO_3 aq., 120 mL; light source: 300 W Xe lamp with a band-pass filter; cell: top-irradiation cell with a Pyrex window.



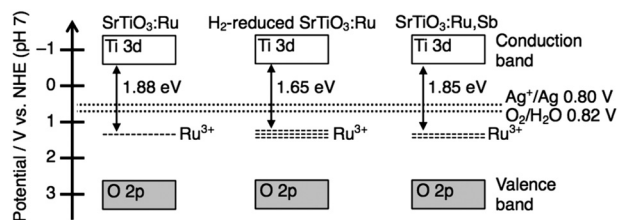


Fig. 5 Proposed band structures of $\text{SrTiO}_3\text{:Ru}$, H_2 -reduced $\text{SrTiO}_3\text{:Ru}$ and $\text{SrTiO}_3\text{:Ru,Sb}$.

excitation of electrons from impurity levels formed by Ru^{3+} to the conduction band formed by $\text{Ti}3d$, the potential of impurity levels formed by Ru^{3+} are estimated to be +1.04 V–+1.27 V vs. NHE at pH 7. The redox potential of Ag^+/Ag and $\text{H}_2\text{O}/\text{O}_2$ are +0.80 V and +0.82 V vs. NHE at pH 7, respectively. Thus, photogenerated electrons in the conduction band and holes at the impurity levels possess thermodynamically enough potential to reduce Ag^+ to Ag and oxidize H_2O to O_2 , respectively. In contrast to this, assuming that the Ru^{3+} -related transition is the excitation of electrons from the valence band formed by $\text{O}2p$ to the impurity levels formed by Ru^{3+} , the potential of the impurity levels are estimated to be +0.71–+0.94 V vs. NHE at pH 7.

These potentials are insufficient to reduce Ag^+ to Ag (+0.80 V vs. NHE). Thus, we can conclude that the sacrificial O_2 evolution from an aqueous AgNO_3 solution proceeded by the excitation from the impurity levels formed by Ru^{3+} to the conduction band of SrTiO_3 . Although the impurity levels are formed by Ru^{4+} , the Ru^{4+} -related absorption does not contribute to the photocatalytic reactions, judging from the action spectra shown in Fig. 4. Sb^{5+} does not form impurity levels in the forbidden band of SrTiO_3 . Thus, the impurity levels formed by Ru^{4+} and Sb^{5+} are not described in Fig. 4 to simplify the band structure relating the photocatalytic reactions.

$\text{SrTiO}_3\text{:Ru,Sb}$ showed higher apparent quantum yields than H_2 -reduced $\text{SrTiO}_3\text{:Ru}$ under light irradiation at around 500 nm, while the former showed lower apparent quantum yields than the latter under light irradiation at around 650 nm, as shown in Fig. 4. The doped Ru was controlled to become Ru^{3+} by both H_2 -reduction and Sb-codoping. The advantage of the Sb-codoping at Ti^{4+} sites is the self-charge compensation due to the formation of Sb^{3+} with an excess amount of Sb_2O_5 in the starting material.⁹ The excessively doped antimony was doped as Sb^{3+} and Sb^{5+} at Ti^{4+} to maintain the charge balance, according to $2\text{Ti}^{4+} = \text{Sb}^{3+} + \text{Sb}^{5+}$. In contrast, oxygen vacancies were formed by H_2 -reduction. Therefore, $\text{SrTiO}_3\text{:Ru,Sb}$ should basically show higher apparent quantum yields than H_2 -reduced $\text{SrTiO}_3\text{:Ru}$ because of less defects. However, the H_2 -reduced $\text{SrTiO}_3\text{:Ru}$ possessed a narrower energy gap than $\text{SrTiO}_3\text{:Ru,Sb}$ resulting in absorption of more photons. Therefore, the H_2 -reduced $\text{SrTiO}_3\text{:Ru}$ showed higher apparent quantum yields than $\text{SrTiO}_3\text{:Ru,Sb}$ at wavelengths close to the absorption edge of H_2 -reduced $\text{SrTiO}_3\text{:Ru}$ at around 650 nm.

There is a negative correlation between the order of the energy gap ($\text{SrTiO}_3\text{:Ru} > \text{SrTiO}_3\text{:Ru,Sb} > \text{H}_2$ -reduced $\text{SrTiO}_3\text{:Ru}$) and the order of the rate of Ru^{3+} ions ($\text{SrTiO}_3\text{:Ru} < \text{SrTiO}_3\text{:Ru,Sb} < \text{H}_2$ -reduced $\text{SrTiO}_3\text{:Ru}$) judging from the ESR spectra (Fig. 1). When the rate of Ru^{3+} increases, the impurity levels formed by Ru^{3+} become wide due to the increased density of states. Accordingly, the energy gap between the conduction band and the impurity levels formed by Ru^{3+} becomes narrow, as shown in Fig. 5. The widened impurity levels are also considered to be favorable for migration of photogenerated holes. Thus, the possible reasons why H_2 -reduced $\text{SrTiO}_3\text{:Ru}$ showed higher activity for the sacrificial O_2 evolution than $\text{SrTiO}_3\text{:Ru}$ and $\text{SrTiO}_3\text{:Ru,Sb}$ are the longest response wavelength and favorable impurity levels for hole migration.

Conclusions

In conclusion, the $\text{SrTiO}_3\text{:Ru,Sb}$ and H_2 -reduced $\text{SrTiO}_3\text{:Ru}$ photocatalysts as well as $\text{SrTiO}_3\text{:Ru}$ showed activities for sacrificial H_2 and O_2 evolution under visible light irradiation. Ru ions were mainly doped as tetravalent Ru in $\text{SrTiO}_3\text{:Ru}$ and the Ru^{4+} ions became Ru^{3+} ions by Sb-codoping and H_2 -reduction. The H_2 evolution activity decreased by controlling Ru to become trivalent, while the O_2 evolution activity increased. Photocatalytic reactions over $\text{SrTiO}_3\text{:Ru}$, $\text{SrTiO}_3\text{:Ru,Sb}$ and H_2 -reduced $\text{SrTiO}_3\text{:Ru}$ proceeded by the excitation from the impurity levels formed by Ru^{3+} to the conduction band of SrTiO_3 . Among them, H_2 -reduced $\text{SrTiO}_3\text{:Ru}$ especially showed the highest O_2 evolution activity and the longest response wavelength up to 750 nm, because of widening of the impurity level formed by Ru^{3+} . Thus, we successfully developed metal oxide photocatalysts with a response to long wavelength visible light (near infrared) by Ru^{3+} doping. This responsive wavelength is almost the longest among those of photocatalysts which are active for O_2 evolution. Thus, Ru-doping will be one strategy to develop metal oxide photocatalysts responding to a wide range of visible light. Moreover, these photocatalysts can be employed as O_2 -evolving photocatalysts in a Z-scheme photocatalyst system.

Conflicts of interest

There are no conflicts to declare.

Acknowledgements

This work was supported by JSPS KAKENHI Grant Numbers 17H06433 and 17H06440 in Scientific Research on Innovative Areas “Innovations for Light-Energy Conversion (I⁴LEC)”, and 17H01217.

References

- 1 F. E. Osterloh, *Chem. Mater.*, 2008, **20**, 35.
- 2 A. Kudo and Y. Miseki, *Chem. Soc. Rev.*, 2009, **38**, 253.



- 3 R. Abe, *J. Photochem. Photobiol., C*, 2010, **11**, 179.
- 4 K. Maeda, *J. Photochem. Photobiol., C*, 2011, **12**, 237.
- 5 T. Yamada and K. Domen, *ChemEngineering*, 2018, **2**, 36.
- 6 S. Chen, Y. Qi, C. Li, K. Domen and F. Zhang, *Joule*, 2018, **2**, 2260.
- 7 A. Kudo, H. Kato and I. Tsuji, *Chem. Lett.*, 2004, **33**, 1534.
- 8 R. Kenta, T. Ishii, H. Kato and A. Kudo, *J. Phys. Chem. B*, 2004, **108**, 8992.
- 9 H. Kato, H. Kobayashi and A. Kudo, *J. Phys. Chem. B*, 2002, **106**, 5029.
- 10 T. Ishii, H. Kato and A. Kudo, *J. Photochem. Photobiol., A*, 2004, **163**, 181.
- 11 R. Niishiro, H. Kato and A. Kudo, *Phys. Chem. Chem. Phys.*, 2005, **7**, 2241.
- 12 A. Iwase and A. Kudo, *Chem. Commun.*, 2017, **53**, 6156.
- 13 S. Suzuki, H. Matsumoto, A. Iwase and A. Kudo, *Chem. Commun.*, 2018, **54**, 10606.
- 14 S. Kawasaki, K. Akagi, K. Nakatsuji, S. Yamamoto, I. Matsuda, Y. Harada, J. Yoshinobu, F. Komori, R. Takahashi, M. Lippmaa, C. Sakai, H. Niwa, M. Oshima, K. Iwashina and A. Kudo, *J. Phys. Chem. C*, 2012, **116**, 24445.
- 15 R. Niishiro, S. Tanaka and A. Kudo, *Appl. Catal., B*, 2014, **150**, 187.
- 16 R. Asai, H. Nemoto, Q. Jia, K. Saito, A. Iwase and A. Kudo, *Chem. Commun.*, 2014, **50**, 2543.
- 17 R. D. Shannon, *Acta Crystallogr., Sect. A: Cryst. Phys., Diffraction, Theor. Gen. Crystallogr.*, 1976, **32**, 751.
- 18 M. Matsumura, M. Hiramoto and H. Tsubomura, *J. Electrochem. Soc.*, 1983, **130**, 326.
- 19 D. E. Scaife, *Sol. Energy*, 1980, **25**, 41.

